International Journal of Heat and Mass Transfer 52 (2009) 5814–5826

Contents lists available at ScienceDirect

International Journal of Heat and Mass Transfer

journal homepage: www.elsevier.com/locate/ijhmt

Nanofiber coating of surfaces for intensification of drop or spray impact cooling

R. Srikar [a], T. Gambaryan-Roisman [b,c], C. Steffes [c], P. Stephan [b,c], C. Tropea [c,d], A.L. Yarin [a,c,*]

[a] Department of Mechanical and Industrial Engineering, University of Illinois at Chicago, 842 W. Taylor St., Chicago, IL 60607-7022, USA
[b] Institute of Technical Thermodynamics, Technische Universität Darmstadt, Petersenstr. 30, 64287 Darmstadt, Germany
[c] Center for Smart Interfaces, Technische Universität Darmstadt, Petersenstr. 32, 64287 Darmstadt, Germany
[d] Institute of Fluid Mechanics and Aerodynamics, Technische Universität Darmstadt, Petersenstr. 30, 64287 Darmstadt, Germany

ARTICLE INFO

Article history:
Received 3 June 2009
Received in revised form 17 July 2009
Accepted 17 July 2009
Available online 16 September 2009

Keywords:
Nanofibers
Drop impact cooling
Heat transfer enhancement

ABSTRACT

A novel enhancement of drop and spray cooling for microelectronic and radiological elements and server rooms requiring extremely high heat fluxes is proposed. The key idea of the method is to cover the heat transfer surfaces with electrospun non-woven polymer nanofiber mats. The mats are permeable for water drops. The enhanced efficiency of drop cooling in the presence of nanofiber mats observed experimentally results from full elimination of receding and bouncing of the drops, characteristic of the current spray cooling technology. Therefore, the drops evaporate completely, and the large cooling potential associated with the latent heat of water evaporation is more fully exploited. This is paradoxical: the best cooling can be provided by a "fur overcoat"! The proposed cooling method alone may lead to a breakthrough in further miniaturization of microelectronic chips, optical and radiological elements and accelerate the development of a new generation of computers. In order to check the suitability of different materials for the drop and spray cooling applications, the thermal and structural properties of nanofiber mats based on four different polymers have been measured over a wide temperature range. Based on the results of these measurements, the most suitable materials have been chosen.

© 2009 Elsevier Ltd. All rights reserved.

1. Introduction

A comprehensive review of various methods for cooling of high-heat flux electronic, optical and radiological devices can be found in the recently published monograph [1]. Miniaturization and breakthrough developments of multiple semiconductor, optical and radiological components are severely hindered by the requirement of cooling such devices at heat fluxes of the order of 1 kW/cm^2 [1,2]. Different approaches to cooling include conduction and heat spreading, air cooling, piezo fans, synthetic jet cooling, ionic wind, liquid jet cooling (including liquid metal jets), heat pipes, cold plates, immersion cooling, micro-channel heat sinks and spray cooling. Among these methods, spray cooling is the most effective [3,4]. However, the efficiency of spray cooling is still far from maximal. Significant receding motion of the spread liquid lamellae on hot metal and silicon surfaces leads in many cases to complete bouncing and interruption of cooling, as well as the Leidenfrost effect. This effect arises due to extremely fast evaporation, leading to drop levitation over the surface rather than contact cooling [5]. Below the Leidenfrost point the spray impact on a hot target is frequently accompanied by formation of a fluctuating liquid film. This film constitutes a significant thermal resistance and therefore prevents high liquid evaporation rates and reduces the cooling efficiency.

A radical improvement of the situation could be achieved if a smart coating would be present on the hot surface. If such a coating at the first moment after a drop impact would act as an impenetrable surface, the drop would spread on it as in an ordinary drop impact onto a dry surface. However, if subsequently the coating would be impregnated by the spread drop lamella and the water would reach the hot surface underneath, drop bouncing and levitation would be completely eliminated. Then, the whole water mass brought by the drop would evaporate in direct contact with the surface. Such a coating would allow an almost complete use of the available latent heat of evaporation for cooling and should result ultimately in high cooling rates. Does such a coating exist? Based on the proof of concept discussed below, the answer is affirmative, and such a coating is provided by an electrospun nanofiber mat of approximate thickness 100 μm.

The advanced applications of nanomaterials ascertain the need for elucidating their particular physical properties. Electrospun nanofiber mats represent a typical example of nanomaterials, which find a wide range of applications in mechanical, chemical and biomedical engineering [6–10]. Electrospinning is a versatile and inexpensive technique for producing robust nanofibers with

* Corresponding author. Address: Department of Mechanical and Industrial Engineering, University of Illinois at Chicago, 842 W. Taylor St., Chicago, IL 60607-7022, USA. Tel.: +1 312 996 3472; fax: +1 312 413 0447.
E-mail address: ayarin@uic.edu (A.L. Yarin).

0017-9310/$ - see front matter © 2009 Elsevier Ltd. All rights reserved.
doi:10.1016/j.ijheatmasstransfer.2009.07.021

Table 1
Electrospinning parameters.

Polymer	Molecular weight (kDa)	Conc. (wt%)	Solvent	Ratio	Electric field strength (kV/cm)	Size (nm)
PCL	80	11	DMF/MC	40/60	~1.4	540
PCL-CB	80	11	DMF/MC	40/60	~1.4	570
PMMA	996	11	DMF	–	~1	1500
PAN	150	12	DMF	–	~1	400
PU	225	10	Ethanol/THF	80/20	~1	600

Table 2
Polymer characteristics.

Polymer	Structure	Glass transition temperature (°C)	Melting point temperature (°C)
PCL	Crystalline [23]	~−60 [22,25]	60 [23]
PMMA	Crystalline [24]	125 [24]*	300 [24]*
PAN	Amorphous [27]	85 [26]	317 [26]
PU	Amorphous*	−40*	175*

* Information provided by the manufacturer.

Table 3
Mass loss.

Polymer	PCL	PCL-CB	PMMA	PAN	PU
Average mass loss (%)	0	0.4854	0.956	6.642	1.2723

diameters in the range 10–10^3 nm, which has already been scaled up to a full industrial level as filter media [11], as well as attracts attention as strain and gas sensors, thermal interfaces in electronic devices, chemical/biological protection layers, and heat management elements [12–15]. The application of electrospun mats for cooling proposed in the present work requires an understanding of their physical properties, in particular under non-isothermal conditions. There are some studies which address thermal behavior of electrospun nanofibers. In particular, rearrangements of crystalline structure of several polymers confined in nanofibers was elucidated using Differential Scanning Calorimetry (DSC), Fourier Transform Infrared (FTIR), and wide-angle X-ray diffraction (WAXD), and efforts were made to link the observed micro-structural changes in crystallinity to mechanical strength of individual nanofibers [16–21]. It was reported that crystallinity in nanofibers is reduced compared to the macroscopic bulk samples of the same polymers because of rapid solvent evaporation and solidification in electrospinning process. Apparently, annealing of nanofibers at elevated temperatures increases their crystallinity toward the levels characteristic of comparable macroscopic bulk polymer samples. Moreover, re-crystallization of the axially-oriented crystallites into radially-oriented crystallites with morphologies characteristic of bulk samples was observed. In [21] the observed DSC thermograms demonstrated identical glass transition and melting temperatures, as well as specific melting enthalpies for Poly(ε-caprolactone) nanofibers and bulk samples. The reported identity most probably stems from the pre-processing applied to the nanofibers in [21], namely compression molding at 50 °C prior DSC measurements. The pre-processing at 50 °C most probably restored the bulk-like structure in PCL. In the present work we show that the Poly(ε-caprolactone), which does not undergo any pre-processing, exhibits a different behavior, as discussed below.

The aim of the present work is in the proof of concept that electrospun nanofiber mats can tremendously facilitate cooling of hot surfaces, which makes them attractive candidates for applications in micro- and optoelectronic and radiological devices (Sections 2 and 3). In addition, we discuss a detailed mechanism responsible for shrinkage of nanofiber mats at elevated temperatures and its relation to the microscopic thermally-induced changes occurring in the polymer crystalline structure (Sections 2 and 4). The thermal behavior of four typical polymers is studied: namely, Poly(ε-caprolactone) (PCL), Poly(methylmethacrylate) (PMMA), Polyacrylonitrile (PAN) and Polyurethane (PU) in electrospun nanofibers and original pellets are studied using Differential Scanning Calorimetry (DSC). The observed micro-structure transformations are discussed in relation to the onset of thermally-induced shrinkage of nanofiber mats, which initially manifests itself as sintering of junctions of the individual nanofibers observed optically. Electrospun nanocomposites of these polymers with Carbon Black (CB) nanoparticles are also considered (Section 4). Conclusions are drawn in Section 5.

2. Experimental

2.1. Materials

The following four polymers used in this study, PCL (M_w = 80 kDa), PMMA (996 kDa), PAN (150 kDa) were purchased from Sigma–Aldrich. Polyurethane elastomer (PU, Tecophilic SP-80A-150) were purchased from Lubrizol. The following solvents were used to prepare polymer solutions for electrospinning: Dimethylformamide (DMF), Dichloromethane (MC), Tetrahydrofuran (THF) and Ethanol (all purchased from Sigma–Aldrich). CB 200 grade carbon black nanoparticles used to electrospin nanocomposite nanofibers were purchased from Cabot Corporation. All the materials were used without any further purification or processing.

Fig. 1. Images of drops deposited on the unheated strip coated with a PAN nanomat. (a) immediately after deposition; (b) 10 min after deposition; (c) 17 min after deposition.

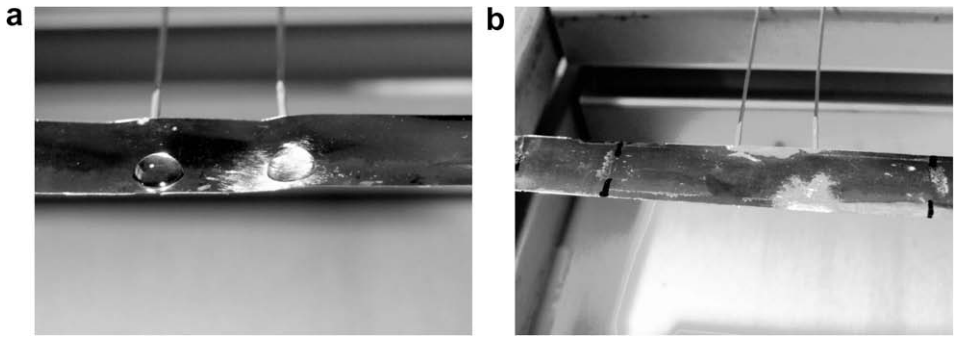

Fig. 2. (a) Two drops gently deposited on an uncoated steel strip. Reflections appear at the region where the surface has been artificially roughened to increase wettability (without much effect). (b) A drop deposited on a steel strip coated with a wettability promoter.

2.2. Electrospinning

A standard electrospinning setup described elsewhere [6,22] was used in this study. The electrospinning conditions are listed in Table 1 together with the as-spun nanofiber sizes (cross-sectional diameters) determined using Olympus-BX51 optical microscope. The PCL-CB composite nanofibers were produced by adding 10%wt CB w.r.t. PCL in the polymer solution. All the polymers were dissolved in their respective solvents and mechanically stirred at 50 °C for around 5 h. All the electrospun mats were collected on a horizontal flat stainless steel plate except for PMMA which was collected on a slow-rotating flat disk. The electrospinning process was carried out under room temperature (24 °C) at a relative humidity of 22–24%. Thickness of deposited nanofiber mats increases linearly with deposition time at the rates about 32 nm/min.

2.3. Drop impact cooling

The drop impact cooling tests have been performed with 10 μm stainless steel strips covered by PAN nanofiber mats. Water drops falling under the action of gravity or gently deposited onto the strip have been used to evaluate cooling effect. For comparison, cooling of an uncoated surface (without nanomat), as well as cooling of a

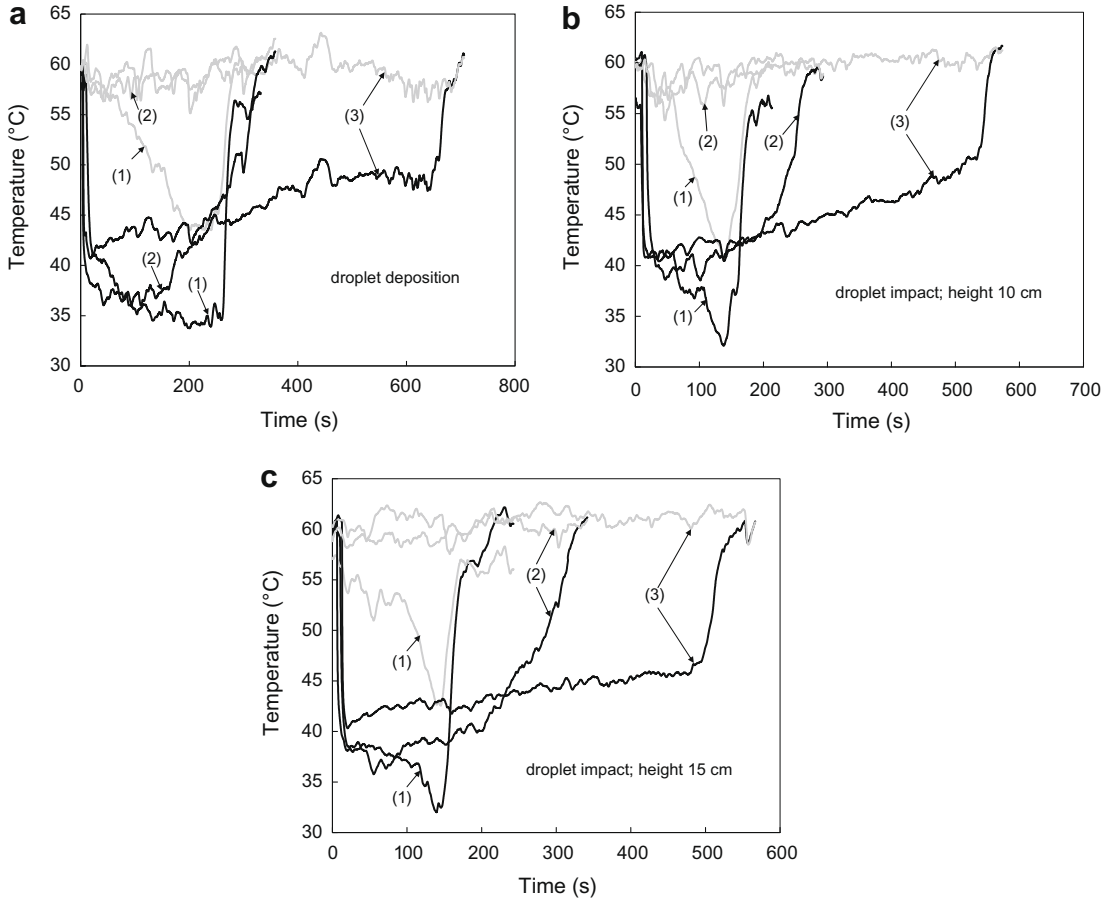

Fig. 3. Evolution of the strip temperatures directly under the deposited (impacted) drop (black lines) and at the distance of 1 cm from it (grey lines); (1) strip coated with PAN nanofiber mat; (2) strip coated with NO DROP fluid to promote wettability; (3) uncoated strip. (a) Gently deposited drop; (b) drop released from the height of 10 cm; (c) drop released from the height of 15 cm. The initial strip temperature was 60 °C in all cases. Drop radii were of the order of 1 mm.

surface coated with the NO DROP fluid (supplied by Röhm) acting as a wettability promoter were studied.

2.4. Thermal analysis

The electrospun nanofiber mats were cut into small almost rectangular pieces and stacked inside Tzero Aluminum pans (Cat. No T081120). The weight of the pieces was between 2 and 4 mg depending on the electrospinning deposition time. The aluminum pans were sealed with their corresponding lids to ensure negligible loss of polymer mass during heating. Differential Scanning Calorimetry was conducted using DSC Q200, TA instruments. The instrument was ramped at 10 °C/min under a constant flow rate of 50 mL/min nitrogen. All the samples were initially equilibrated at 20 °C before their thermal analysis had been started. A similar procedure was adopted in the case of bulk pellets of the same polymers. The thermal and structural properties of the bulk polymers in the pellets found in literature are listed in Table 2. All the experiments were carried out twice to ensure reproducibility.

2.5. Mass loss analysis

Pieces of electrospun nanofiber mats were stacked as described in Section 2.4. They were weighed using a SARTORIUS LE26P Microbalance. Then, the mats were heated to various temperatures (in the range 24–150 °C) for 15 min each and weighed once again. The heating was carried out in an open atmosphere. The results are shown in Fig. 7 and Table 3. All measurements were repeated twice to ensure reproducibility.

2.6. Optical analysis of nanofiber mats during heat treatment

The electrospun nanofiber mats were cut into rectangular pieces and placed on a glass slide. The glass slide was subjected to elevated temperatures and the surface temperature was measured using OMEGA HH23 microprocessor thermocouple. The optical images of the nanofiber mats taken during heat treatment are shown and discussed in Section 4.

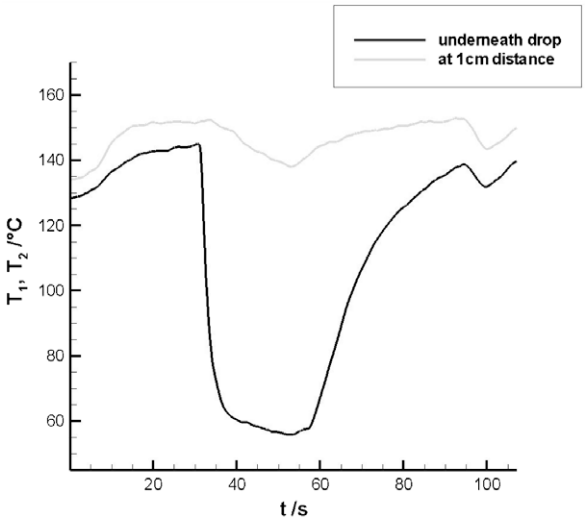

Fig. 4. Evolution of the strip temperatures directly under the impacted drop (black line) and at the distance of 1 cm from it (grey line). The strip was coated with PAN nanofiber mat.

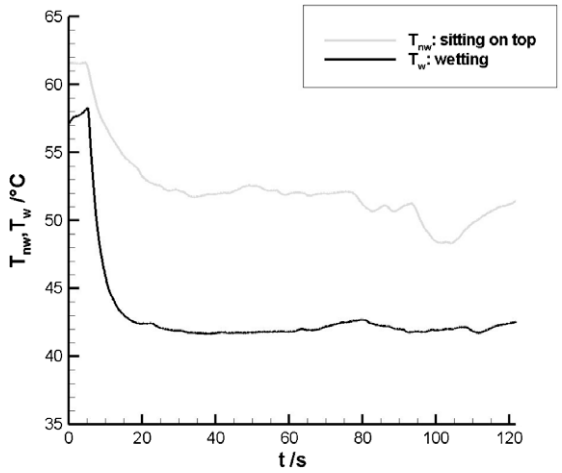

Fig. 5. "Skeletal" Leidenfrost effect. The black curve shows reduction of the strip temperature when water reached the steel surface through the PAN nanomat. The grey curve shows a lesser cooling when droplet evaporates on a thicker nanomat without direct contact with the strip underneath. The initial strip temperature was about 60 °C in this case. Both temperature histories were recorded by a thermocouple underneath the location of the drop impact.

3. Intensification of drop impact cooling by using the nanofiber mat coating

Cooling performance was investigated by examining water drops impacting onto heated 10 μm stainless steel strips. The first strip has been covered by PAN nanomat comprised of randomly oriented nanofibers. The second strip has been tested without any coating, and the third strip has been coated with a wettability promoter (NO DROP fluid). After a gentle deposition of a drop onto an unheated strip coated with a PAN nanomat, a very high contact angle has been observed (Fig. 1a). After several minutes water begins to penetrate into the nanomat (Fig. 1b and c). Initially the nanomat acts effectively as a super-hydrophobic surface, since most of its bulk is just air (the porosity is of the order of 90% and the pores are filled with air). The PAN nanofiber material is typically partially wettable with the contact angle values close to 30–40. Therefore, it takes a relatively long time until weak wettability and the gravity force result in a partial impregnation of such mats by gently deposited water drops.

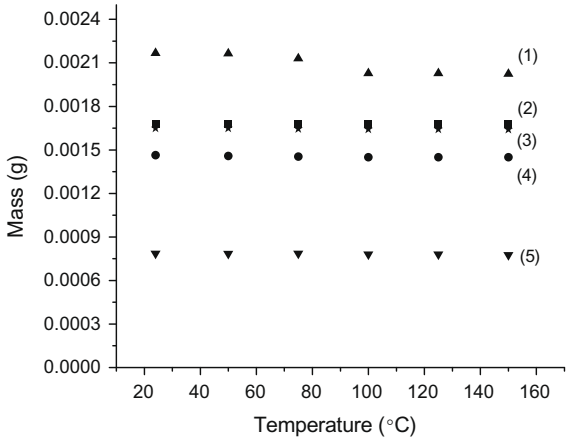

Fig. 6. Masses of polymer nanofiber mats at room temperature and after 15 min heat treatment at different temperatures. (1) PAN, (2) PCL, (3) PCL-CB, (4) PMMA, and (5) PU. The data error bars are ±2 μg.

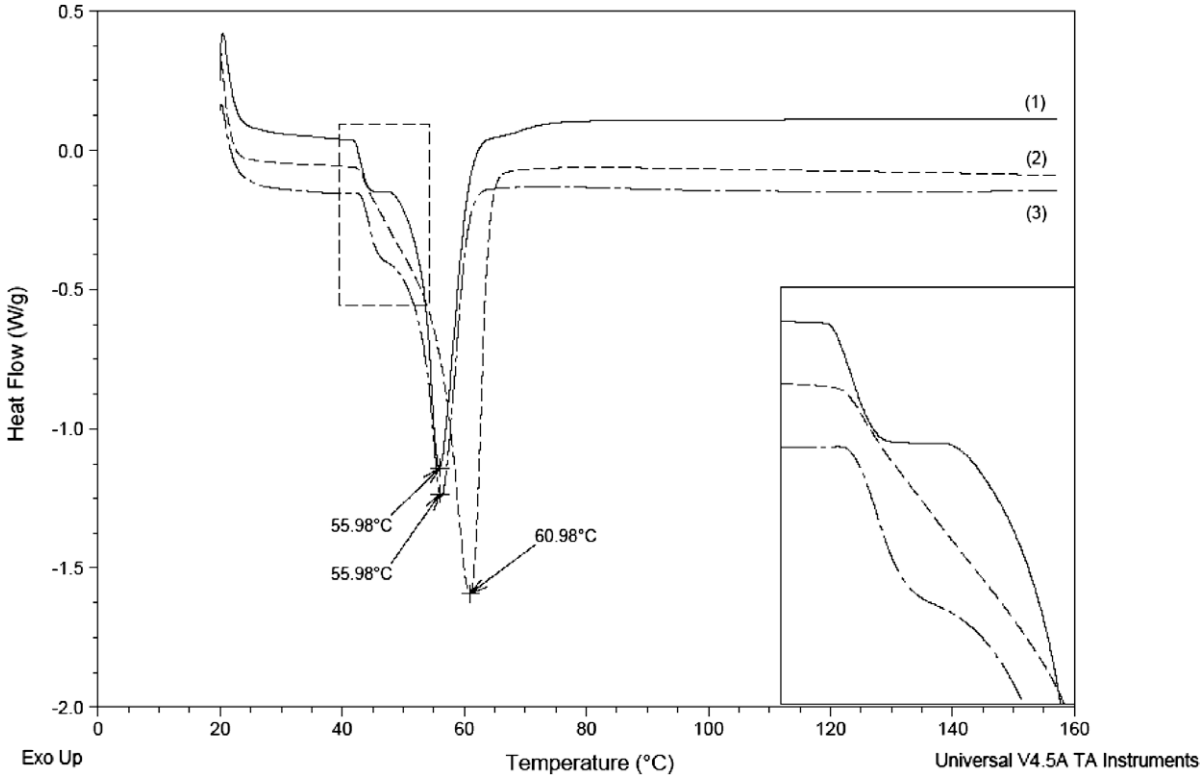

Fig. 7. DSC thermograms for PCL. (1) PCL nanofiber electrospun from 11% solution; (2) PCL pellet; (3) PCL-CB nanocomposite nanofiber mat. The data corresponding to the rectangular frame on the left are scaled up in the rectangle on the right.

The shapes of the drops gently deposited on an unheated strip without coating and the strip with the NO DROP coating are shown in Fig. 2a and b, respectively. It is seen that the wettability of the uncoated steel surface is rather poor, whereas it is significantly improved after the application of the wettability promoter.

For the heat transfer experiments, two K-type thermocouples have been attached to the back side of each strip (seen in Figs. 1

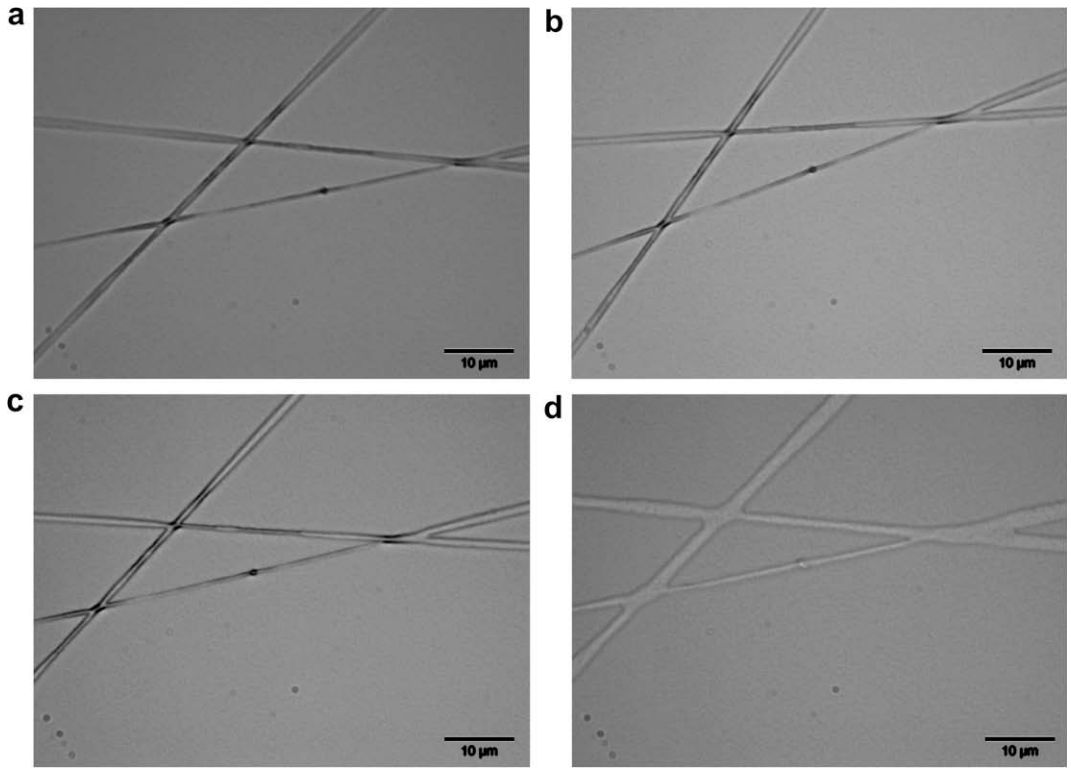

Fig. 8. Optical images of junctions of individual PCL nanofibers at different temperatures. (a) 36.5, (b) 49.3, (c) 53.55, (d) 59.9 °C.

and 2) 1 cm apart. In all the heat transfer experiments the strips have been heated by an electric current with an average constant power so that the initial temperature measured by both thermocouples was about 60 °C in the first series of the experiments. In the second series, it was increased to about 140 °C. After the achievement of steady temperature values, the cooling experiments were conducted. In the first experiment a water drop with a diameter of about 3 mm has been gently deposited exactly above the left thermocouple. The temperature measurements of both thermocouples have been recorded until the drop has completely evaporated. In the second experiment, a similar drop fell down from a height of 10 cm and impacted the strip at the location of the left thermocouple. In the third experiment, a similar drop fell down at the location of the left thermocouple from the height of 15 cm. The measurements were repeated with the drop deposition/impact over the location of the right thermocouple as well, to check the reproducibility. The data acquisition started immediately before the deposition (or release) of the drops.

The results of the temperature measurements are shown in Fig. 3. Fig. 3a depicts the results obtained after a gentle drop deposition, Figs. 3b and c show the results obtained with drop falling down from the heights of 10 and 15 cm, respectively. The black lines represent the temperature histories measured directly under the location of drop impact (deposition), and the grey lines represent the corresponding temperature histories measured at the distance of 1 cm from the drop impact location. It is clearly seen from Figs. 3a–c that the deposition (impact) of a single drop on a nanomat-coated strip reduces the strip temperature at least at the distance of 1 cm from the location of drop deposition (impact), which results from the water sucking and spreading in the capillary structure and evaporation. This property suggests that in the case of spray impact, a highly uniform cooling of the surface can be easily achieved.

It is seen from the figure that the minimal temperature achievable by droplet deposition (impact) onto a nanomat-coated strip is about 8 °C lower than in the case of the drop impact onto an

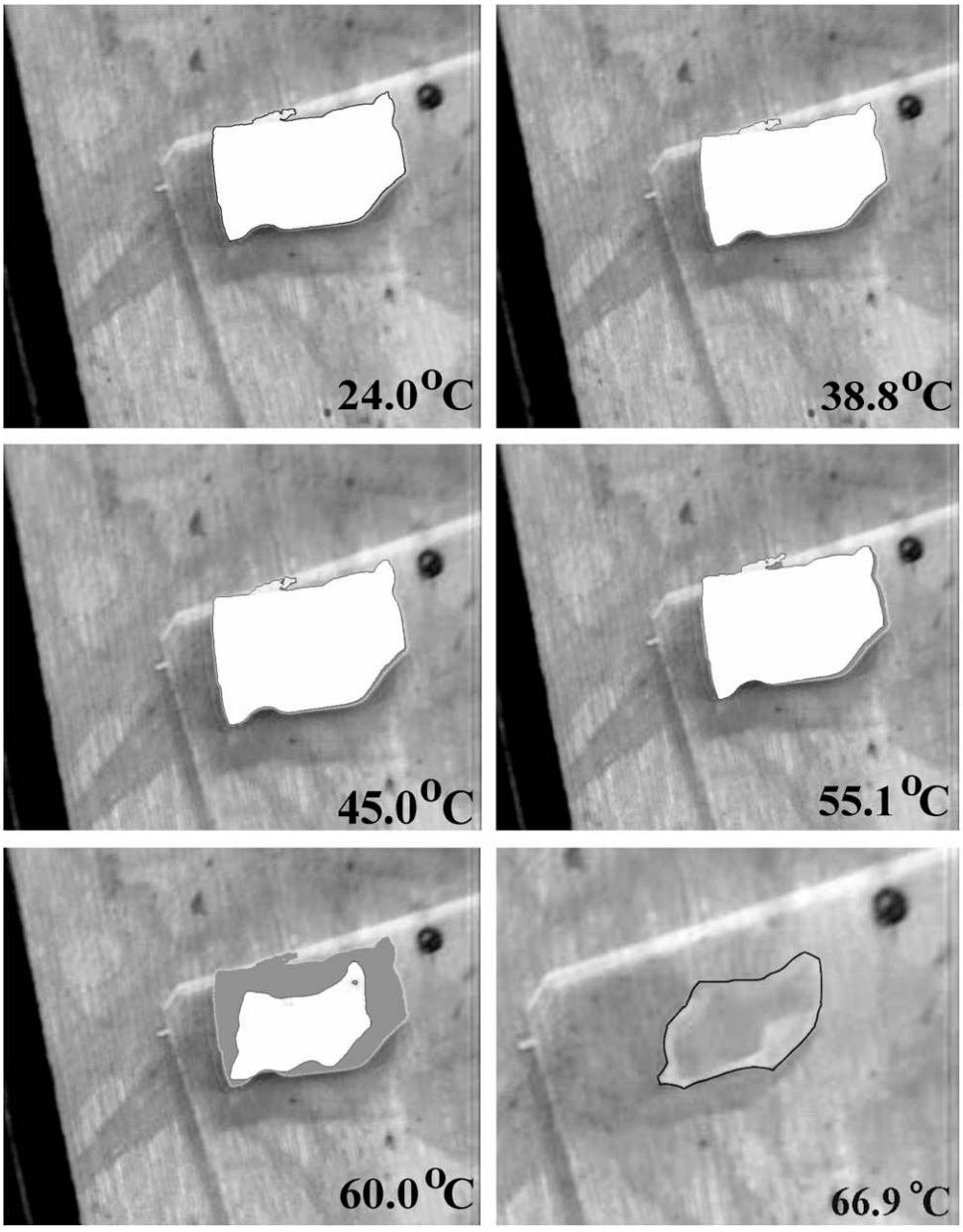

Fig. 9. Optical images of electrospun PCL nanofiber mats at various temperatures.

uncoated strip and up to 6 °C lower than in the case of the drop impact onto a strip coated with the wettability promoter. These results show the superiority of the cooling performance by drop impact (deposition) onto the nanomat-coated substrate. Note, that in this case the overall temperature reduction under the nanomat is about 28 °C. Nanomats possess porosity of the order of 90% [6]. They effectively fence water inside and prevent drop receding. Moreover, since wet nanomats consist mostly of water, thermal conductivity of fibers plays a secondary role compared to that of the latent heat of water evaporation.

The time needed for complete drop evaporation is approximately equal to the time during which the cooling effect (temperature reduction below 60 °C) is measurable (about 150 s in Fig. 3b and c). It is clearly seen from Figs. 3a–c that the evaporation time of a drop on a nanomat-coated strip is up to three times shorter than that on an uncoated strip. For the gently deposited drop, the drop evaporation time on a nanomat-coated strip is only slightly shorter than that for the strip coated with the wettability promoter. However, with increasing height of the drop release (and therefore the drop impact velocity), the difference in drop evaporation time between the nanomat-coated strip and the strip with wettability promoter coating increases.

It should be noted that in the case of a multiple drop impact the maximal attainable cooling rate is determined by the product of the total mass flow of the spray and the latent heat of evaporation. This cooling rate is achieved if each impacting droplet is completely evaporated, or, in other words, if the impact of each droplet onto a certain location happens after a complete evaporation of the previous droplet. Therefore, the shorter the evaporation time is the more droplets per unit time may impact the surface and completely evaporate; the achievable overall cooling rate can be increased.

Fig. 4 shows the results obtained at the high initial temperature (about 140 °C) of a strip. In this case after the drop impact on the PAN mat from the height of about 20 cm, the temperature is rapidly reduced by about 80 °C. The duration of the drop evaporation is about $\Delta t = 20$ s, which is more than seven times shorter that in the case of the initial strip temperature of 60 °C. At the same time, only a slight temperature reduction has been registered by the second thermocouple at a distance of 1 cm throughout the whole observation time (see Fig. 4). This indicates that the drop evaporates before it spreads to the radius of 1 cm. The measured value of Δt allows an estimate of the heat flux q at the location of drop impact under an assumption that the droplet did not spread significantly upon impact. Namely, the heat flux is estimated as the ratio of the latent heat adsorbed by complete evaporation of the droplet and the droplet projection area and the evaporation time: $q = \frac{\rho 4/3\pi a^3 L}{\pi a^2 \Delta t} = \frac{4\rho a L}{3\Delta t}$, where ρ and L are the water density and latent heat and a is the drop radius. Taking for the estimate $a = 1$ mm and $\Delta t = 20$ s (as in Fig. 4), we obtain $q \approx 15$ W/cm^2. It should be noted that the removed heat flux in the present experiments has been limited by the maximal power achieved by electrical heating of a thin steel foil. It is expected that in setups allowing higher heating rates, the drops will evaporate faster, resulting in correspondingly higher rates of heat removal by evaporation.

Nanofiber mats thicker than approximately 100 μm prevent drop penetration to the strip surface. However, even in this case a certain cooling effect is possible (Fig. 5), which is attributed to a "skeletal" Leidenfrost effect. In such cases drops evaporate at the nanomat surface, which cools nanofibers, and through the nanofiber skeleton, heat is removed from the hot strip underneath (in contrast to the regular Leidenfrost effect, where without a skeleton, indirect cooling is practically impossible).

4. Thermal and structural properties of nanofiber mats

The results of Section 3 show that polymer nanofiber mats represent promising coatings which can significantly reduce substrate

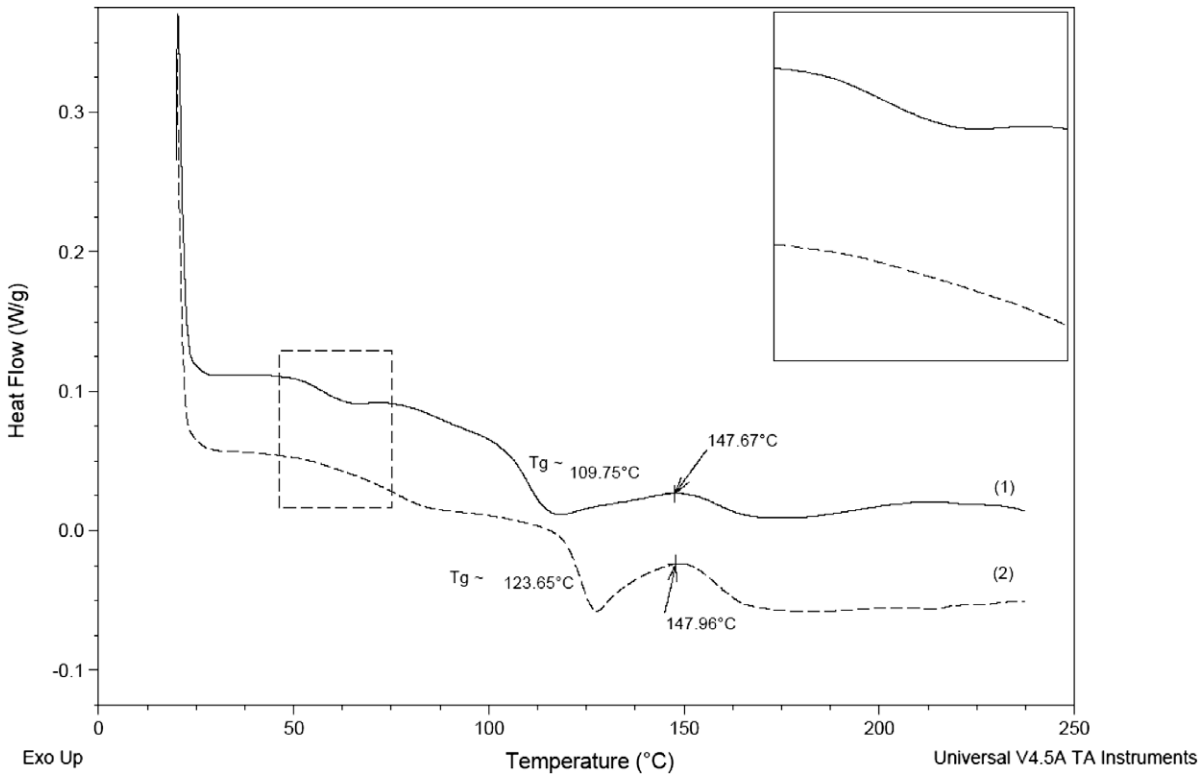

Fig. 10. DSC thermograms for PMMA. (1) PMMA nanofibers electrospun from 11% solution; (2) PMMA powder. The data corresponding to the rectangular frame on the left is scaled up in the rectangle on the right.

temperature when water spray cooling is used. Microelectronic equipment is typically sustained at temperatures below 100 °C. Then, the question arises regarding which electrospun nanofiber mats can sustain their nanoporous structure without melting and shrinking in the temperature range of 20–100 °C. It is emphasized that this question cannot be addressed only using data on glass transition and melt temperature of the corresponding bulk polymers, since it is expected that these characteristics are reduced in nanomaterials, in particularly in nanofiber mats. The present Section addresses this question for PCL, PCL-CB, PMMA, PAN and PU nanofiber mats.

Fig. 6 shows masses of polymer nanofiber mats measured at room temperature and after 15 min heat treatment at different temperatures. The corresponding mass losses averaged over the whole temperature range are listed in Table 3. The average mass losses after the heat treatment for PCL, PCL-CB, PMMA and PU mats do not exceed 1–1.5%. On the other hand, PAN mats lost about 7% of their mass in average. Fig. 6 elucidates that most of the mass losses in PAN mats occurs in the range of 75–100 °C. This is further corroborated by DSC analysis for PAN discussed below.

The DSC thermograms for PCL nanofiber mats and pellets are shown in Fig. 7. These include (1) PCL nanofiber mat electrospun from 11% PCL solution, (2) PCL pellet and (3) electrospun PCL-CB nanocomposite nanofiber mat. The DSC thermograms for PCL show several features. First, there is a significant reduction in the melting point of electrospun PCL nanofibers and nanocomposite PCL nanofibers compared to that of PCL pellet, in distinction from the results for PCL reported in [21] where the nanofibers were compressively molded at 50 °C prior DSC measurements. The data in Fig. 7 show that melting point reduced from 60.9 °C for PCL pellets to 56 °C for PCL nanofibers. The decrease in the melting temperature may be attributed to three phenomena previously mentioned in the literature: (i) high surface to volume ratio of the electrospun fibers, (ii) plasticizing effect of a residual solvent in the nanofiber mats on the polymer chains and (iii) modification of the crystalline structure as a result of rapid solidification of polymer solutions in electrospinning. Our data, however, attribute the third phenomenon to the developments observed in Fig. 7 around 42 °C. At this temperature both types of the nanofibers demonstrate a visible thermal signature of realignment of macromolecular chains and possible crystallization well before melting. DSC was also used to measure crystallinity. DSC software has an inbuilt feature to measure the crystallinity of a substance. It is the ratio of the heat of fusion responsible for melting of the substance to that of the reference material, which in this case was pure PCL pellets. The electrospun PCL nanofibers had 66.28% crystallinity, which is also characteristic of the PCL pellets. It is emphasized that the glass transition temperature of PCL is around −60 °C [21]. Therefore, with no observable baseline shift, the phenomena occurring with PCL nanofibers around 42 °C cannot be attributed to glass transition. The DSC thermograms for PCL are accompanied by optical observations of junctions of individual nanofibers caught on a glass slide moved above the ground electrode. The junctions were observed at different temperatures and the results for PCL are depicted in Fig. 8. The observable deformations of the nanofibers begin near to their junctions around 50 °C. They clearly exhibit smoothening due to the action of surface tension (which is largest at the junctions where local curvature of material is very large), which results in viscous creeping flow of softened polymer. Such flow can accompany structural rearrangements of macromolecular chains in re-crystallization up to the ultimate crystalline melting close to 56 °C. The morphological changes depicted in Fig. 8 clearly correspond to the wavy depressions in the DSC thermograms for nanofibers seen in Fig. 7. The optical images in Fig. 8 show deformation near the nanofiber junctions and change in optical image contrast indicating apparent melting between 53 and 60 °C, although no overall observable features could be seen below below 45 °C (cf. Fig. 9).

The presence of CB nanoparticles in PCL nanofibers slightly shifts the corresponding DSC thermogram toward that of PCL pellets in Fig. 7. CB nanoparticles also altered the molecular rearrangement, as the data in Fig. 7 show, whereas the melting temperature remained practically the same as for pure PCL nanofibers.

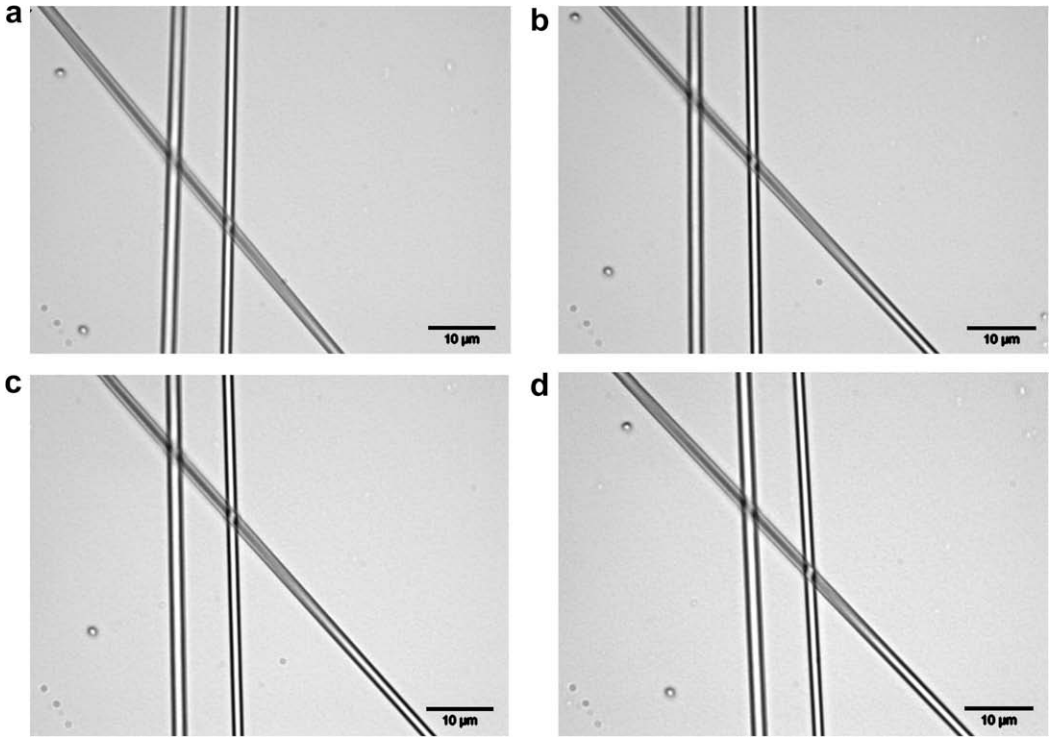

Fig. 11. Optical images of junctions of individual PMMA nanofibers at different temperatures. (a) 33.3, (b) 50.9, (c) 90.7, (d) 125.7 °C.

The measured crystallinity in PCL-CB nanofibers was found to be 64.9%, almost the same as in PCL nanofibers. The thermal treatment of bulk PCL-CB fibers showed results similar to pure PCL fiber mats.

The optical images of the PCL nanofiber mats during heat treatment are shown in Fig. 9. Mat shrinkage is illustrated by the shrinkage of the white area on the grey background corresponding to the sample at room temperature. The visible overall changes in the PCL nanofiber mats begin at 45 °C (Fig. 9). At 66.9 °C the sample was completely molten. Clearly, PCL nanofiber mats (with or without CB nanoparticles) cannot be used in spray cooling of microelectronics components above 45 °C, i.e. are practically inappropriate.

The DSC thermograms for (1) PMMA nanofiber mats electrospun from 11%wt solution and (2) PMMA powder are shown in Fig. 10. PMMA is a crystalline polymer and electrospinning reduces crystallinity due to rapid evaporation of solvent and solidification of the polymer. Crystallinity of PMMA nanofibers was determined via DSC and found to be 50.15% compared to that of PMMA powder. The inset in Fig. 10 shows a "dip" at 60 °C in the thermogram for PMMA nanofibers. This feature is absent in the thermogram for PMMA powder. The "dip" clearly results from the annealing of nanofibers, which leads to an increase in crystallinity. Therefore, this "dip" in the thermogram should be attributed to molecular rearrangement of PMMA chains within nanofibers at 60 °C (a phenomenon similar to the one observed in the thermogram of PCL nanofibers around 40 °C). For PCL nanofibers such rearrangement happens well above the glass transition and is followed by melting. On the contrary, for PMMA nanofibers, the rearrangement and recrystallization of polymer chains happens before the glass transition. Indeed, the thermogram for PMMA nanofibers in Fig. 10 shows glass transition at 109 °C, which is much earlier than for PMMA powder (the glass transition at 124 °C, Fig. 10). The decrease in the glass transition temperature of PMMA nanofibers corresponds to their lower crystallinity compared to that of PMMA powder. At still higher temperatures, both PMMA nanofibers and PMMA powder probably undergo a depolymerization/degradation

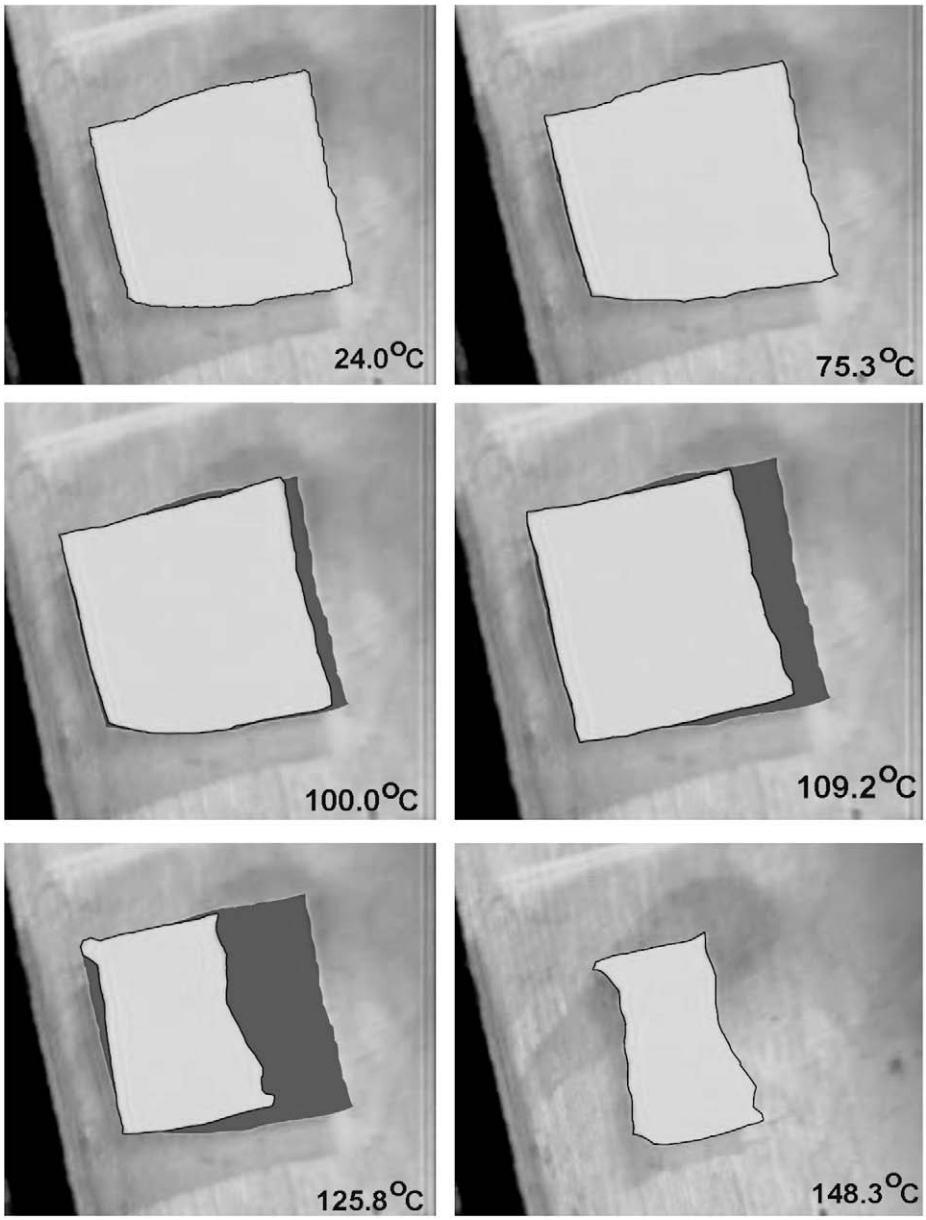

Fig. 12. Optical images of an electrospun PMMA nanofiber mat as temperature increases.

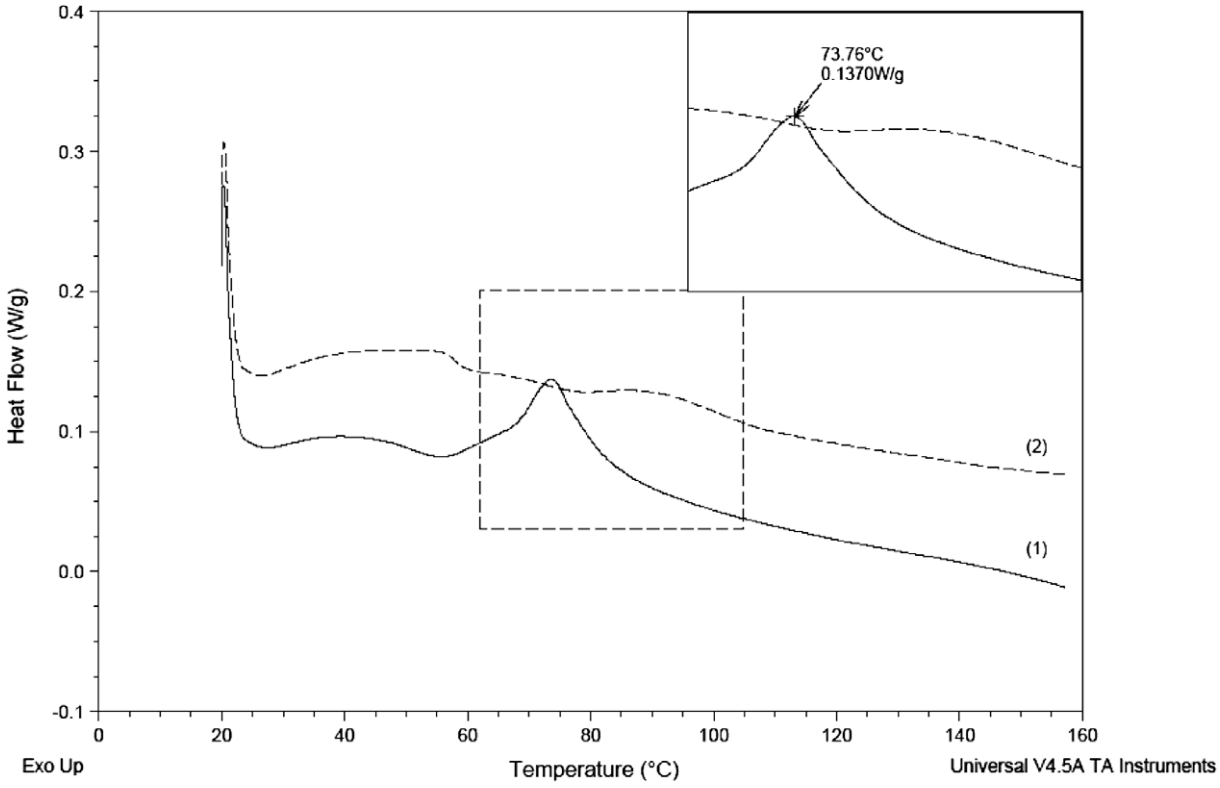

Fig. 13. DSC thermograms for PAN. (1) PAN nanofibers electrospun from 12% solution; (2) PAN powder.

around the same temperature of 148 °C (Fig. 10). This observation probably indicates that the glass transition temperature might be the threshold point where the internal structure and properties of the electrospun PMMA nanofibers match up with those of the PMMA powder. The optical images of the junctions of PMMA nanofibers at different temperatures are shown in Fig. 11. It shows

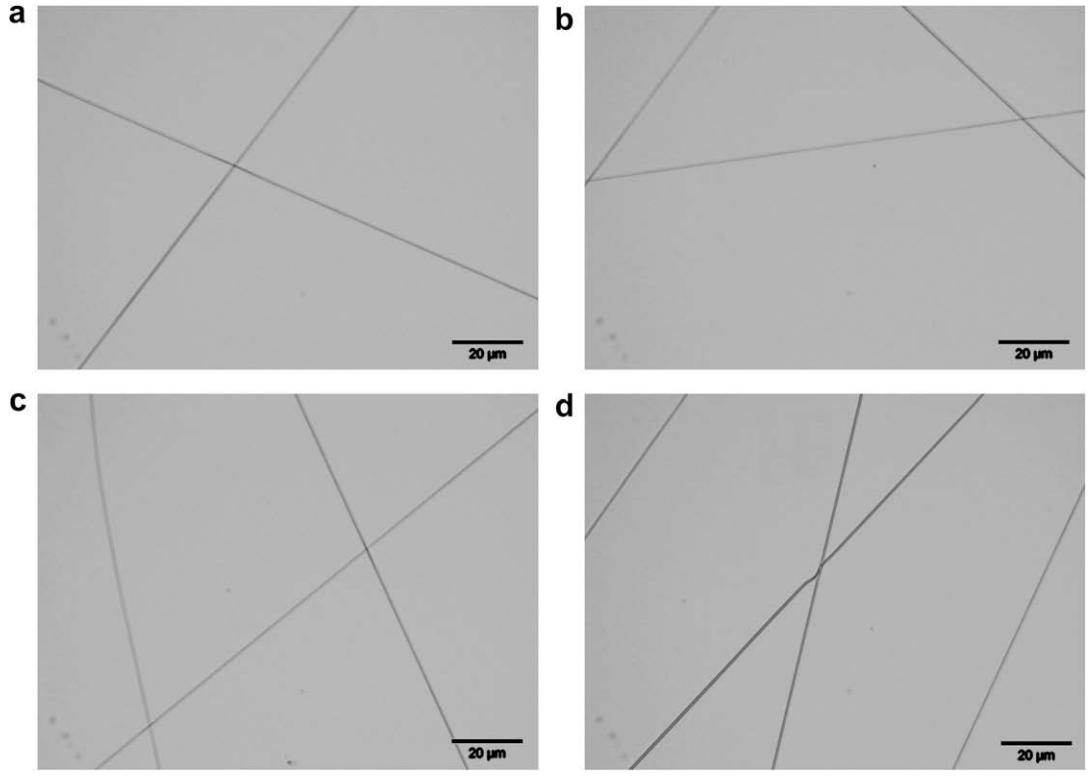

Fig. 14. Optical images of junctions of individual PAN nanofibers at different temperatures. (a) 35.3, (b) 68.1, (c) 90.1, (d) 125.0 °C.

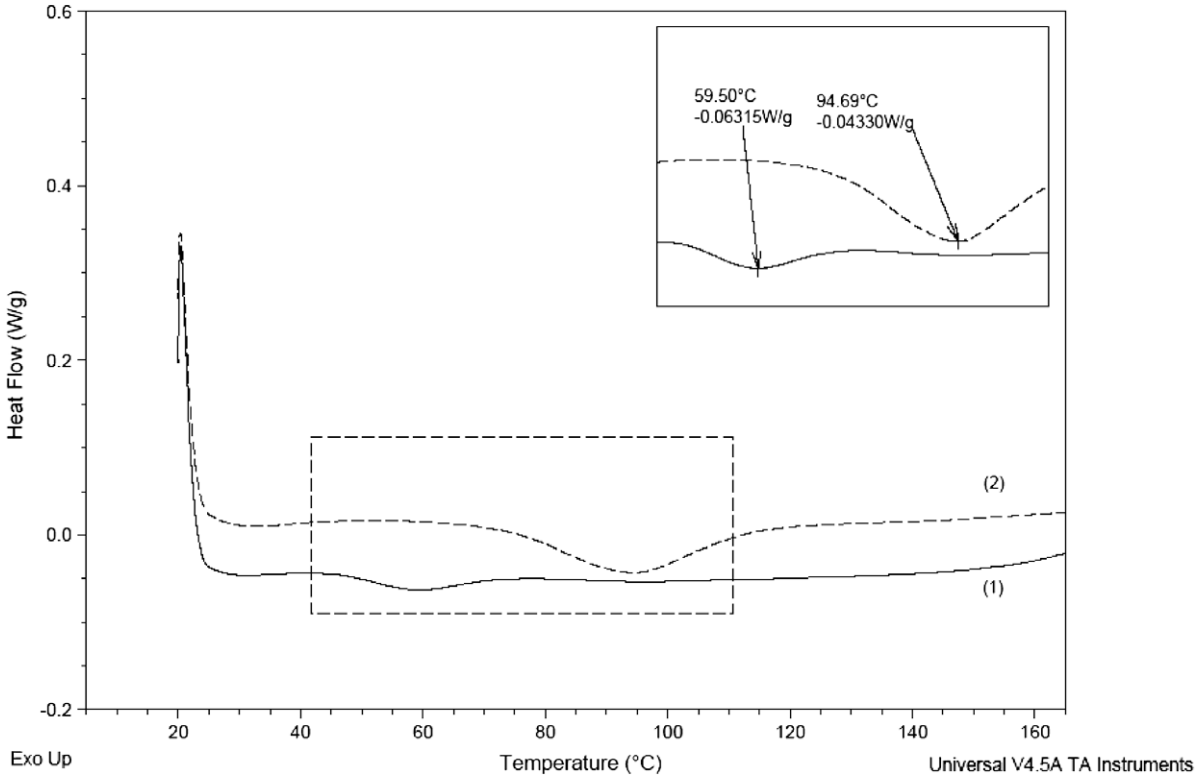

Fig. 15. DSC thermograms for PU. (1) PU nanofibers electrospun from 10% solution; (2) PU pellet.

that neither macromolecular rearrangement and re-crystallization, nor glass transition do not produce any visible sintering-like flow even in the locations of high curvature near nanofiber junctions.

The optical images of a PMMA nanofiber mat during heating are shown in Fig. 12. Shrinkage of the grey area over the black one illustrates the sample evolution compared to its initial configura-

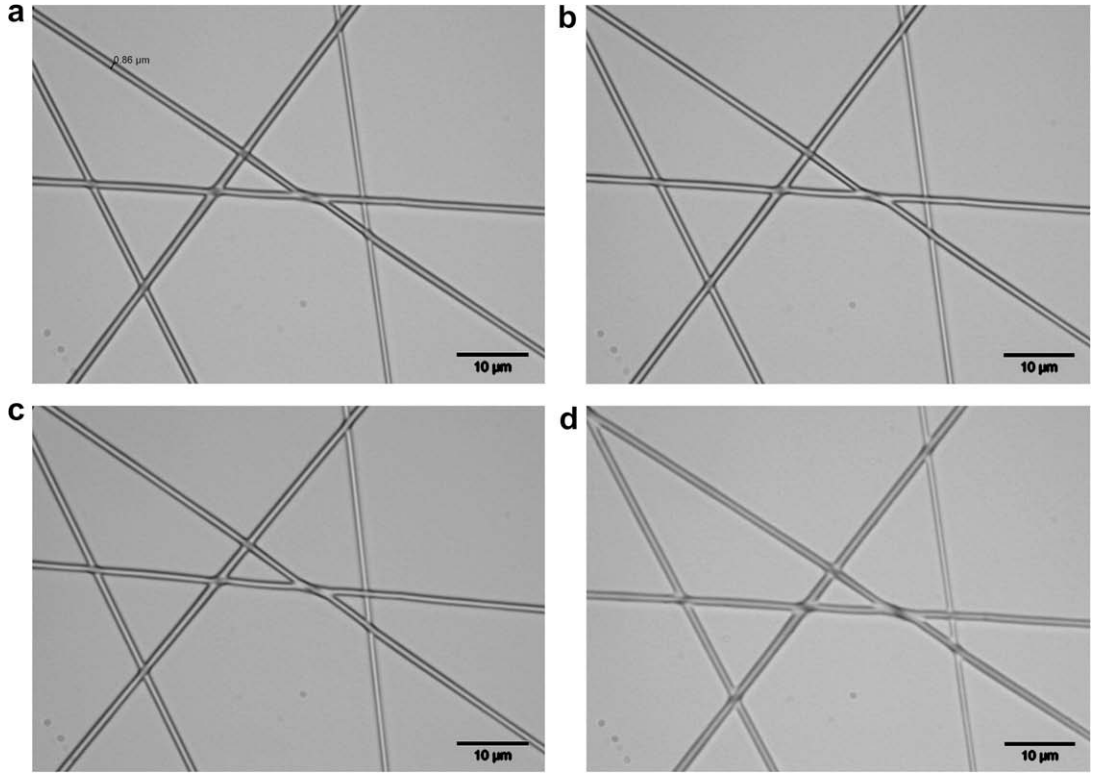

Fig. 16. Optical images of junctions of individual PU nanofibers at different temperatures. (a) 26.7, (b) 40.8, (c) 53.8, (d) 87.5 °C.

tion. The last frame in Fig. 12 at 148.3 °C depicts the final mat configuration. It is possible to use PMMA nanofiber mats in spray cooling of microelectronics systems up to 100 °C.

The DSC thermograms for PAN nanofibers electrospun from a 12% solution and for PAN powder are shown in Fig. 13. The figure demonstrates an exothermal peak with specific heat release of about 0.137 W/g around 73.76 °C for the PAN nanofiber mat in distinction from PAN powder. The results for PAN shown in Fig. 6 and Table 3 suggest a significant mass loss around this temperature. However, our DSC procedure does not allow any mass losses. Therefore, the exothermal peak can be attributed only to a change in the specific heat at constant volume, $c_{v,}$ of the specimen. The reason for the above-mentioned mass losses and change of specific heat may be due to (i) a partial degradation of PAN nanofibers around this temperature or to (ii) a chemical reaction. Each of these processes might be triggered by oxidation process at the tremendous nanofiber surface. The optical images of several individual PAN nanofibers are shown in Fig. 14. It shows no observable changes in the PAN nanofiber crossbars around 73.76 °C. Only at a much higher temperature (~125 °C) a minor bending near the junction is visible in Fig. 14d. The overall images of PAN nanofiber mats (not shown here), however, did not show any observable changes for any temperature up to 150 °C. This makes PAN nanofiber mats fully appropriate for spray cooling systems in microelectronics in the whole temperature range of interest.

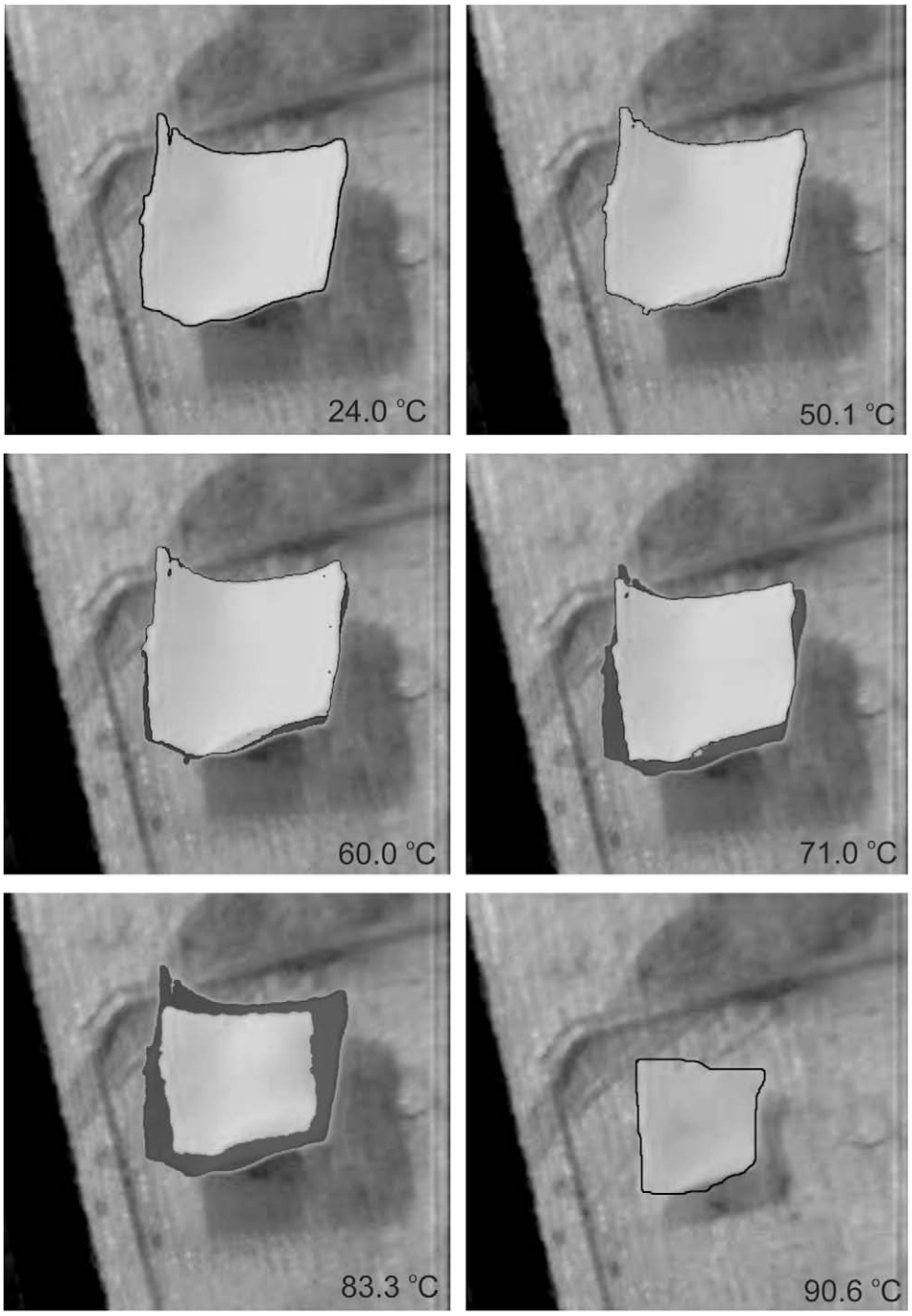

Fig. 17. Shrinkage of an electrospun PU nanofiber mat at elevated temperatures.

The DSC thermograms for PU are shown in Fig. 15. Depressions in the thermograms are visible for both nanofiber and pellets, however, at different temperatures. The depressions are interpreted as molecular chain rearrangements. PU nanofibers begin to undergo such rearrangement at a lower temperature of about 50 °C compared to PU pellets (about 85–90 °C). Shift of the rearrangement to a lower temperature in PU nanofibers is similar to the correspondent phenomena observed for PCL and PMMA nanofibers. At higher temperatures the PU nanofiber thermogram is similar to that of PU pellet. The PU thermograms also showed crystallization, but at a higher temperature (around 210 °C) for both nanofibers and pellets (not shown in Fig. 15).

The optical images of the PU nanofiber junctions in Fig. 16 show that sintering-like flow begins above 60 °C. The overall images of the PU nanofiber mats subjected to heat treatment shown in Fig. 17 reveal a considerable shrinkage/creep as the temperature exceeds 50 °C. Therefore, PU nanofiber mats cannot be used in the spray cooling systems in microelectronics at temperatures above 50 °C, i.e. are practically irrelevant.

5. Conclusions

The work introduces a novel idea of spray cooling of micro- and optoelectronic components and radiological devices using polymer nanofiber mats coating on heating elements. The concept sounds paradoxical, since these air-filled, practically non-wettable porous materials might be better expected to be effective thermal insulators rather than facilitate cooling. Nevertheless, the reality is different. Water drops easily penetrate them even under the action of gravity and definitely on impact. A water drop, which spreads inside a nanofiber mat, can never recede or bounce back, as happens in spray cooling of uncoated metal, polymer and silicon surfaces. Therefore, such drops inside nanofiber mats are fully evaporated in close contact with the warm substrate and remove a significant amount of heat due to very high latent heat of water evaporation. The heat transfer results in this work represent a proof of concept and demonstrate superiority of the proposed method of cooling using electrospun nanofiber mats over cooling of uncoated surfaces or surfaces coated with a wettability promoter. For example, for a substrate with an initial temperature of 60 °C, a direct impact of a single water drop (as in the current spray cooling methods) reduced the surface temperature to about 41 °C, whereas an impact on an approximately 100 μm PAN nanomat-to about 33 °C.

A thorough investigation of the thermal and structural properties of several nanomats in the temperature range 20–100 °C revealed that PAN and PMMA nanofiber mats are fully appropriate for microelectronic applications, whereas PCL and PU nanofiber mats are not.

Acknowledgements

R. S. and A.L.Y. are grateful for partial support of their work by National Science Foundation through Grant NIRT CBET-0609062. T.G.-R. wishes to acknowledge the financial support of DFG (German Science Foundation) through the Emmy Noether-Program and the cluster of Excellence 25 g.

References

[1] L.P. Yarin, A. Mosyak, G. Hetsroni, Fluid Flow, Heat Transfer and Boiling in Micro-Channels, Springer, Berlin, 2009.
[2] I. Silverman, A.L. Yarin, S.N. Reznik, A. Arenshtam, D. Kijet, A. Nagler, High heat-flux accelerator targets: cooling with liquid metal jet impingement, Int. J. Heat Mass Transfer 49 (17–18) (2006) 2782–2792.
[3] M. Fabbri, S. Jiang, V.K. Dhir, A comparative study of cooling of high power density electronics using sprays and microjets, J. Heat Transfer – Trans. ASME 127 (1) (2005) 38–48.
[4] I. Mudawar, Assessment of high-heat-flux thermal management schemes, IEEE Trans. Compon. Packag. Technol. 24 (2) (2001) 122–141.
[5] A.L. Yarin, Drop impact dynamics: splashing, spreading, receding, bouncing..., Annu. Rev. Fluid Mech. 38 (2006) 159–192.
[6] D.H. Reneker, A.L. Yarin, E. Zussman, H. Xu, Electrospinning of nanofibers from polymer solutions and melts, Adv. Appl. Mech. 41 (2007) 43–195.
[7] A.L. Yarin, E. Zussman, J.H. Wendorff, A. Greiner, Material encapsulation and transport in core–shell micro/nanofibers, polymer and carbon nanotubes and micro/nanochannels, J. Mater. Chem. 17 (25) (2007) 2585–2599.
[8] D.H. Reneker, A.L. Yarin, Electrospinning jets and polymer nanofibers, Polymer 49 (10) (2008) 2387–2425.
[9] A. Greiner, J.H. Wendorff, Electrospinning: a fascinating method for the preparation of ultrathin fibers, Angew. Chem. Int. Ed. 46 (30) (2007) 5670–5703.
[10] A. Greiner, J.H. Wendorff, Functional sef-assembled nanofibers by electrospinning, Adv. Polym. Sci. 219 (2008) 107–171.
[11] Y. Filatov, A. Budyka, V. Kirichenko, Electrospinning of Micro- and Nanofibers. Fundamentals and Applications in Separation and Filtration Processes, Begell House, New York, 2007.
[12] X. Wang, W. Wang, X. Li, B. Carlberg, X. Lu, Z. Cheng, J. Liu, D. Shangguan, Investigation of dielectric strength of electrospun nanofiber based thermal interface material, in: Proceedings of the 2007 International Symposium on HDP apos, Issue 26–28, pp. 1–6.
[13] P.W. Gibson, C. Lee, F. Ko, D.H. Reneker, Application of nanofiber technology to nonwoven thermal insulation, J. Eng. Fibers Fabr. 2 (2) (2007) 32–40.
[14] X.B. Yan, Z.J. Han, Y. Yang, B.K. Tay, NO2 gas sensing with polyaniline nanofibers synthesized by a facile aqueous/organic interfacial polymerization, Sens. Actuators B 123 (1) (2007) 107–113.
[15] M.K. Tiwari, A.L. Yarin, C.M. Megaridis, Electrospan fibrous nanocomposites as permeable, flexible strain sensors, J. Appl. Phys. 103 (4) (2008) 044305.
[16] Y. Liu, L. Cui, F. Guan, Y. Gao, N.E. Hedin, L. Zhu, H. Fong, Crystalline morphology and polymorphic phase transitions in electrospun nylon-6 nanofibers, Macromolecules 40 (17) (2007) 6283–6290.
[17] V. Thomas, M.V. Jose, S. Chowdhury, J.F. Sullivan, D.R. Dean, Y.K. Vohra, Mechano-morphological studies of aligned nanofibrous scaffolds of polycaprolactone fabricated by electrospinning, J. Biomater. Sci. – Polym. Ed. 17 (9) (2006) 969–984.
[18] E.H. Jeong, S.S. Im, J.H. Youk, Electrospinning and structural characterization of ultrafine poly(butylene succinate) fibers, Polymer 46 (23) (2005) 9538–9543.
[19] X. Zong, K. Kim, D. Fang, S. Ran, B.S. Hsiao, B. Chu, Structure and process relationship of electrospun bioabsorbable nanofiber membranes, Polymer 43 (16) (2002) 4403–4412.
[20] T. Subbiah, G.S. Bhat, R.W. Tock, S. Parameswaran, S.S. Ramkumar, Electrospinning of nanofibers, J. Appl. Polym. Sci. 96 (2) (2005) 557–569.
[21] S.C. Wong, A. Baji, S. Leng, Effect of fiber diameter on tensile properties of electrospun poly(epsilon-caprolactone), Polymer 49 (21) (2008) 4713–4722.
[22] D.H. Reneker, A.L. Yarin, H. Fong, S. Koombhongse, Bending instability of electrically charged liquid jets of polymer solutions in electrospinning, J. Appl. Phys. 87 (9) (2000) 4531–4547.
[23] D. Nava, C. Salom, M.G. Prolongo, R.M. Masegosa, Thermal properties and interactions in blends of poly(epsilon-caprolactone) with unsaturated polyester resins, J. Mater. Process. Technol. 143 (Special Issue, SI) (2003) 171–174.
[24] Material Safety Data Sheet (MSDS) PCL ($M_w \sim 80$ kDa) Sigma–Aldrich.
[25] Material Safety Data Sheet (MSDS) PMMA ($M_w \sim 996$ kDa) Sigma–Aldrich.
[26] C. Polo Fonseca, F. Cavalcante Jr., F.A. Amaral, C.A. Zani Souza, S. Neves, Thermal and conduction properties of a PCL-biodegradable gel polymer electrolyte with LiSlO4, LiF3CSO3, and LiBF4 salts, International Journal of Electrochemical Science 2 (1) (2007) 52–63.
[27] Material Safety Data Sheet (MSDS) PAN ($M_w \sim 150$ kDa) Sigma–Aldrich.